Catalysis Letters 30 (1995) 201–212

Failure mechanisms of ceramic membrane reactors in partial oxidation of methane to synthesis gas

S. Pei, M.S. Kleefisch, T.P. Kobylinski, J. Faber, C.A. Udovich

Amoco Research Center, Naperville, IL 60566, USA

V. Zhang-McCoy, B. Dabrowski

Physics Department, Northern Illinois University, DeKalb, IL 60115, USA

U. Balachandran, R.L. Mieville and R.B. Poeppel

Energy Technology Division, Argonne National Laboratory, Argonne, IL 60439, USA

Received 16 June 1994; accepted 21 October 1994

In the course of generating synthesis gas (H_2, CO) from methane, we have observed two types of fractures occurring on the Sr(Co, Fe)O_x-type oxygen membrane reactors. The first type occurred shortly after the reaction started and the second type often occurred days after the reaction. To determine the causes of these fractures, we have examined the starting material and fractured membranes using a combination of X-ray diffraction and thermogravimetric analyses. We found that the first type of fracture was the consequence of an oxygen gradient in the membrane, pointing from the reaction side to the air side. This causes a lattice mismatch inside the membrane, leading to fracture. The second type of fracture, however, was the result of a chemical decomposition. We found that the Sr(Co, Fe)O_x-type membrane had been reduced to $SrCO_3$, and elemental Co and Fe by the synthesis gas generated in the reaction. The decomposition causes enormous expansion leading to a large crack along the axis of tube.

Keywords: synthesis gas; methane; perovskite; oxygen permeable membrane

1. Introduction

Although natural gas reserves already exceed ever-diminishing liquid reserves, only a small fraction of natural gas is being used as feedstock in the petrochemical industries. Over the past several years, extensive efforts have focused on the direct and indirect conversion of methane, the most abundant component of natural gas, to value-added products, particularly towards easily transportable fuels [1–4]. Direct routes involve partial oxidation of methane to methanol and/or formaldehyde, or oxidative coupling to ethylene and ethane. Indirect routes include the

reforming of methane to synthesis gas with subsequent application of Fischer–Tropsch technology, which provides paraffin waxes and mid-distillate fuels [5].

Indirect routes involving synthesis gas formation are usually energy intensive (steam reforming is highly endothermic). Direct partial oxidation routes are usually not very selective. Although the partial oxidation of methane to synthesis gas is a potential alternative to today's steam reforming processes, downstream processing requirements cannot tolerate nitrogen (recycle with cryogenic separations is required) and pure oxygen must be used. The most significant cost associated with partial oxidation is that of the oxygen plant.

Ceramic oxygen membrane reactors represent a technology that offers potential in eliminating a separate oxygen plant that is needed by the partial oxidation of methane. A simple configuration of such reactors consists of a tubular membrane with air passing over the outside of the tube and methane through the inside, as illustrated in fig. 1. The membrane is permeable to oxygen at high temperature, but not to nitrogen or any other gas. Consequently, only oxygen in air can be transported to the inside of the reactor, where it reacts with methane to generate partial oxidation products.

Using an apparatus similar to that in fig. 1, we have demonstrated the concept of ceramic oxygen membrane reactors. Here, the ceramic oxygen membrane was made of a perovskite-like material of $Sr(Co_{0.8}Fe_{0.2})O_x$, which is known to exhibit extremely high oxygen permeabilities (two orders of magnitudes over that of stabilized zirconia) at high temperature [6]. The hollow ceramic tubes (6 mm o.d. and 4 mm i.d.) of this oxide were fabricated using an extrusion method [7]. These tubes were then used in our partial oxidation studies to transport oxygen for synthesis gas generation in conjunction with a precious metal reforming catalyst. Although our experimental results supported the oxygen transport concept with successful

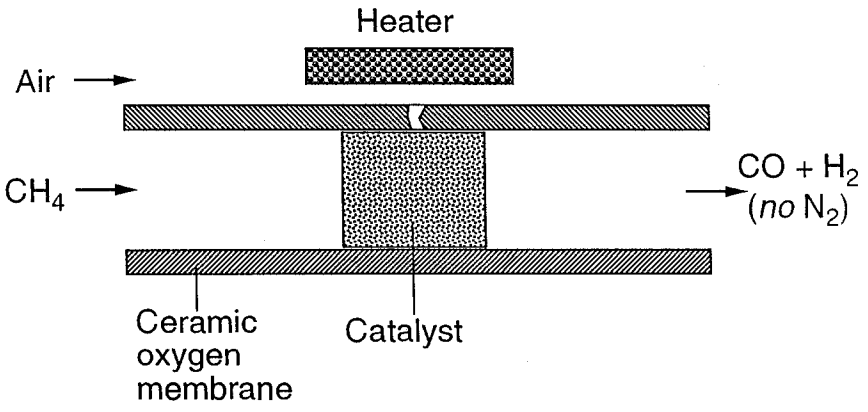

Fig. 1. Schematic drawing of a simple membrane reactor for methane conversion. The location of the first type of fracture is indicated (see text).

utilization towards preferred oxidation, the integrity of the tube diminished with time on stream, eventually leading to catastrophic failure.

The fractures observed can be divided into two categories. The first type occurred shortly (within 1 h) after the reaction started, and the tube in the hot reaction zone (~ 800°C) often broke into many a small piece. The second type occurred long after initiation of the reaction, and a large crack was formed parallel to the axis of the tube. In addition, the previously homogeneous tube showed two shells with different colors: a shining outer shell and a black inner shell, as shown in fig. 2. The present paper addresses the investigation into the reasons why this particular perovskite ceramic membrane material failed under partial oxidation conditions.

2. Experimental

The samples used in this work were prepared by the solid-state reaction of $SrCO_3$, $Co(NO_3)_2 \cdot 6H_2O$ and $Fe(NO_3)_3 \cdot 9H_2O$.

Thermogravimetric analysis (TGA) data were taken on a Cahn TGA171 system. The starting sample for TGA was about 0.5 g in weight and was obtained by fast cooling the material from 1100°C in air. Oxygen partial pressure ($p(O_2)$) inside the TGA apparatus was controlled by the gas mixture of O_2 and Ar. The TGA data were taken during the cooling of the samples from 850°C to room temperature. To ensure that these results were representative of the equilibrium values, the samples were first equilibrated at 850°C and a slow rate (about 0.6°C/min) of cooling was used. Hydrogen reduction was conducted using a gas mixture of 25% H_2 and 75% Ar.

Room-temperature X-ray diffraction (XRD) was carried out on a Scintag PAD V powder diffractometer. In situ XRD was carried out on a Scintag PAD X, theta–theta vertical goniometer powder diffractometer equipped with a Buehler high-temperature furnace and gas handling apparatus. To ensure that the sample

Fig. 2. Photograph of a used membrane reactor tube for synthesis gas generation. Air was flowing outside of the tube while methane and reaction products were flowing inside the tube.

was in a close equilibrium condition with the environment, successive runs were often taken until no further changes in XRD patterns were observed. The thermal expansions of the material were measured during the cooling of a sample. All data were taken using the Cu Kα radiation. A high-purity intrinsic Ge energy dispersive detector was used to minimize high backgrounds due to sample fluorescence.

3. Results and discussion

It was our speculation that the first type of fracture observed might result from a phase change or some unusual lattice expansion of the material during the reaction. As a result, we have examined the high-temperature phase behavior of $Sr(Co_{0.8}Fe_{0.2})O_x$.

The first step of our work was to determine the oxygen content of $Sr(Co_{0.8}Fe_{0.2})O_x$ as a function of temperature and $p(O_2)$. The oxygen content of the starting material was determined by hydrogen reduction. The weight of the sample in the hydrogen-containing atmosphere decreased rapidly with temperature and then reached a plateau at 800°C, with 13% weight loss. XRD analysis showed that the TGA sample cooled down from the plateau consisted of two phases: an element iron phase and the $Sr(OH)_2 \cdot H_2O$ phase. We attributed the latter to the reaction of SrO with moisture in air. This result led us to conclude that during hydrogen reduction the starting material underwent the following decomposition:

$$Sr(Co_{0.8}Fe_{0.2})O_x \rightarrow SrO + 0.8Co + 0.2Fe + [(x-1)/2]O_2(gas),$$

and the decomposition was completed upon reaching the plateau. Based on the above equation and the weight loss at the plateau (13%), the oxygen content of the starting material was determined to be $x = 2.62$. The oxygen contents of the material at other temperatures and $p(O_2)$'s were subsequently calculated from the weight loss with respect to the starting material. The results for 100, 15 and 1% O_2 are plotted in fig. 3, along with the result for Ar.

An inspection of fig. 3 showed that the oxygen content change of $Sr(Co_{0.8}Fe_{0.2})O_x$ contained two features that could be harmful to the integrity of a tube made from this material. First, a cusp occurs in the 1% O_2 curve near 800°C. This is an indication that some phase change might take place in $Sr(Co_{0.8}Fe_{0.2})O_x$ at high temperature. This phase change could create strain leading to the fracture of tubes.

The second feature that is of concern is the change of the oxygen content with $p(O_2)$. The difference of oxygen content between pure oxygen and Ar is nearly 0.1 at 800°C and becomes larger at lower temperatures. Although such difference is required for driving oxygen permeation, it could be a potential problem for integrity of the tube. In principle, the unit cell volume of the material changes with its oxygen content, and as a result, the material on the air side should have a lattice

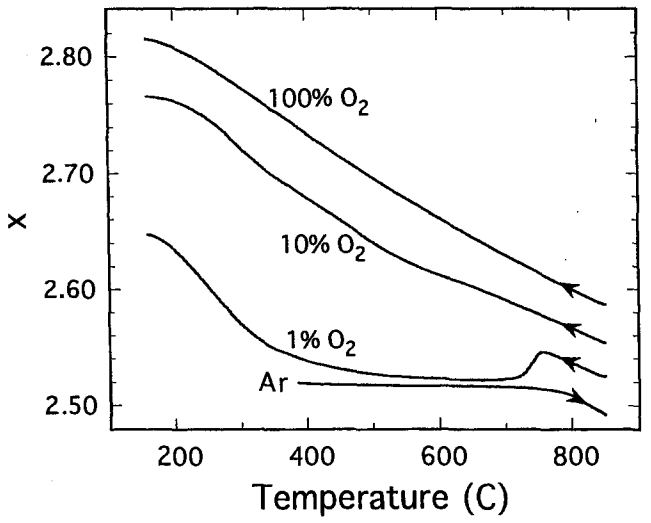

Fig. 3. The oxygen content, x, of $Sr(Co_{0.8}Fe_{0.2})O_x$ as a function of temperature in various O_2–Ar mixtures. The data for 100, 10 and 1% O_2 were taken during slow cooling while the data for Ar were taken during a non-equilibrium heating process.

parameter different from that on the reaction side. This may create sufficiently large strain leading to the fracture of the membrane.

The second step of our work was to explore the structural phase behavior directly with in situ XRD. We were particularly interested in searching for phase changes at high temperature and in determining the dependence of lattice parameters on temperature and $p(O_2)$.

The phase change of $Sr(Co_{0.8}Fe_{0.2})O_x$ at the fixed temperature of 800°C as a function of $p(O_2)$ is shown in fig. 4. The switching sequence of the gas flowing through the sample chamber is as follows:

$$\text{air} \rightarrow 10\%\ O_2 \rightarrow 5\%\ O_2 \rightarrow 1\%\ O_2 \rightarrow N_2 \rightarrow \text{air}.$$

The purpose of switching back to air in the end was to check for the reversibility of any phase change.

At the temperature of 800°C, the material has a simple cubic phase in both air and 10% O_2. However, after the gas is switched to 1% O_2 and N_2, the material transformed into a relatively complex phase. The transition was completely reversible since the XRD pattern taken in air after the transition is essentially identical to that taken in air before the transition. The material at 5% O_2 consisted of a mixture of the two phases.

The complex phase occurring at low $p(O_2)$ was identified to isostructural to $Sr_2Fe_2O_5$ [8–10], $SrCoO_{2.5}$(HT) [11], $Sr(Co_{0.5}Fe_{0.5})O_{2.5}$ [12] and $Sr(Co_{0.8}Fe_{0.2})O_x$ (quenched from HT) [13]. All of them have the brownmillerite-type structure with orthorhombic lattice parameters: $a = \sqrt{2}\,a^*, b = 4a^*$, and $c = \sqrt{2}\,a^*$, where

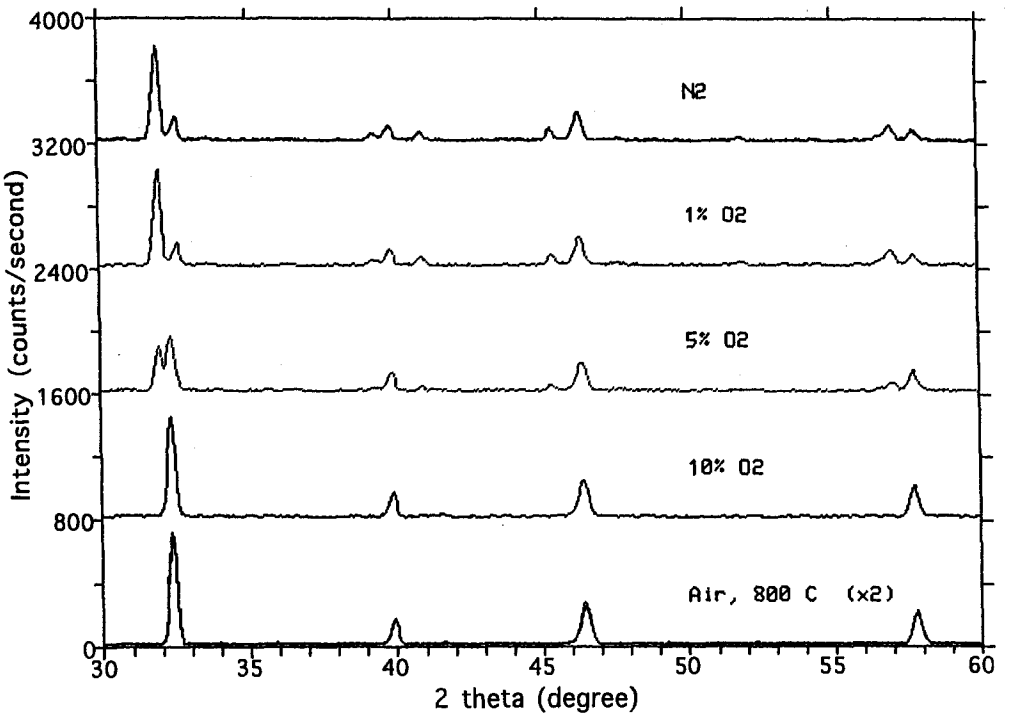

Fig. 4. In situ XRD patterns taken at 800°C in various O_2–N_2 mixtures.

a^* ($\sim$ 3.9 Å) is the pseudo-cubic lattice parameter. The volume of this unit cell is about eight times that of the pseudo-cubic cell.

An inspection of fig. 4 shows that the material expands substantially after the cubic-to-orthorhombic phase transition. This can be seen from the shift of the Bragg peak near $2\theta = 32°$. Evidently, the peak in the orthorhombic phase is located towards the low angle (or larger d-spacing) side of the corresponding peak in the cubic phase. Detailed analysis by Rietveld refinement [14] shows that on an average, the dimension of the orthorhombic unit cell expands by 1% compared with that of the cubic cell. This result suggests that the material inside the tube will expand about 1% in length more than that on the outside. Such a large strain was likely to be the cause for the fracture of the tubes that was encountered in the reactor tests.

Over the temperature range studied, the material remained to be cubic in air and orthorhombic in N_2. Temperature-dependence of the average pseudo-cubic lattice parameters is shown in fig. 5. The lattice parameters for N_2 are consistently greater than those for air at the same temperatures. The differential increases from 1% at high temperature to 1.5% at room temperature. It is thus expected that operating at low temperature could lead to greater strain and more breakage of tubes.

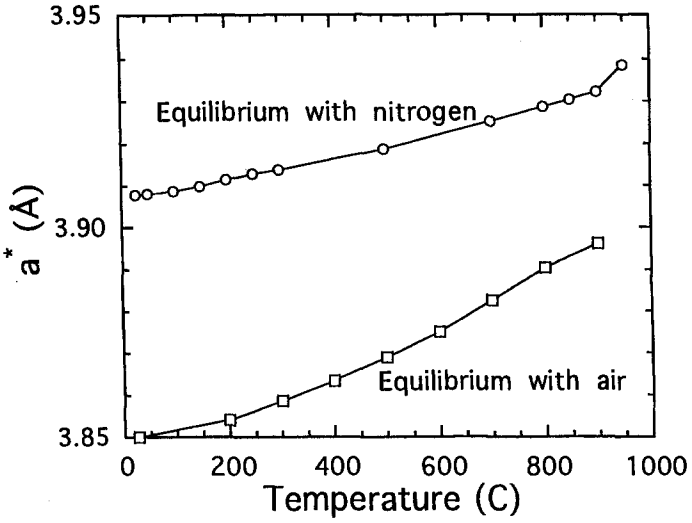

Fig. 5. Average pseudo-cubic lattice parameters, a^*, of $Sr(Co_{0.8}Fe_{0.2})O_x$ as a function of temperature in air and N_2. The material in air has a cubic perovskite structure and a^* is identical to that of the cubic lattice parameter. The material in N_2 has the brownmillerite-type structure and a^* is defined to be $\sqrt{V/8}$, where V is the volume of the orthorhombic unit cell. The data were taken during cooling.

The thermal expansion of $Sr(Co_{0.8}Fe_{0.2})O_x$ in air is nearly twice of that in N_2, as shown in fig. 6. Such behavior is understandable realizing that the overall thermal expansion of an oxygen deficient material contains two components: one that is caused by the temperature change and one that is caused by the change of oxygen content. The oxygen content of the $Sr(Co_{0.8}Fe_{0.2})O_x$ material does not vary substan-

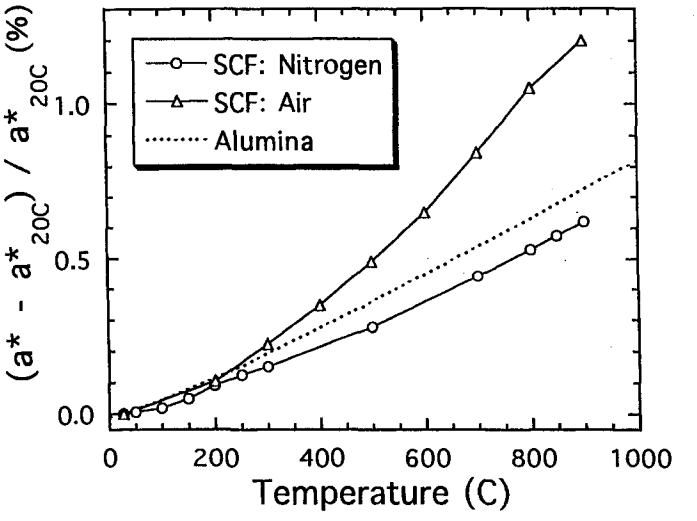

Fig. 6. Average thermal expansion of $Sr(Co_{0.8}Fe_{0.2})O_x$ as a function of temperature in air and N_2. The data were taken during cooling. The dotted line is that of alumina [15].

tially in N_2 ($\sim$ 2.5, referring to fig. 3). Accordingly, the thermal expansion contains only the first component, which had a similar magnitude to that of alumina. When heated in air, however, the material lost a substantial fraction of oxygen ($\Delta x \approx 0.2$, referring to fig. 3), causing the thermal expansion nearly twice of that in N_2.

The thermal expansion in the orthorhombic phase is quite anisotropic, as shown by fig. 7. The *b*-axis (perpendicular to the basal plane) is elongated at a very large rate while the *a*- and *c*-axes (on the basal plane) remain almost constant.

Based on the results of TGA and XRD, we have a clear picture about the state of the $Sr(Co_{0.8}Fe_{0.2})O_x$ tube under reaction conditions. Before the tube was brought up to high temperature, it had an uniform distribution of oxygen with $x \approx 2.7$. Upon heating, the tube began to lose oxygen that was incorporated previously in the fabrication process. However, the material on the inner wall should lose more oxygen compared with that on the outer wall. As a result, a stable oxygen gradient is generated.

It follows that the material, depending on where it is in the tube, may have different phase constituents. A phase representation of the tube at 800°C is proposed, as shown in fig. 8. The tube has the cubic phase in the outer shell and the orthorhombic phase in the inner shell. In addition, there may also exist a middle shell consisting of a mixture of the two phases. Evidently, the least permeable shell will limit the oxygen flux permeating through the membrane. Measurements by Kruidhof et al. [16] suggested that the oxygen permeabilities of the orthorhombic phase were smaller than those of the cubic phase. Therefore, the inner shell is likely to be the flux-limiting one.

As a result of the oxygen gradient and the phase changes, a large lattice mis-

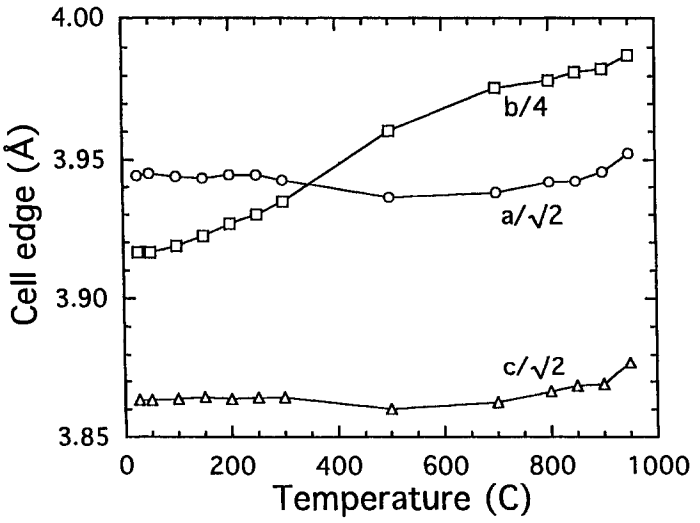

Fig. 7. Orthorhombic lattice parameters of $Sr(Co_{0.8}Fe_{0.2})O_x$ as a function of temperature in N_2. The data were taken during cooling.

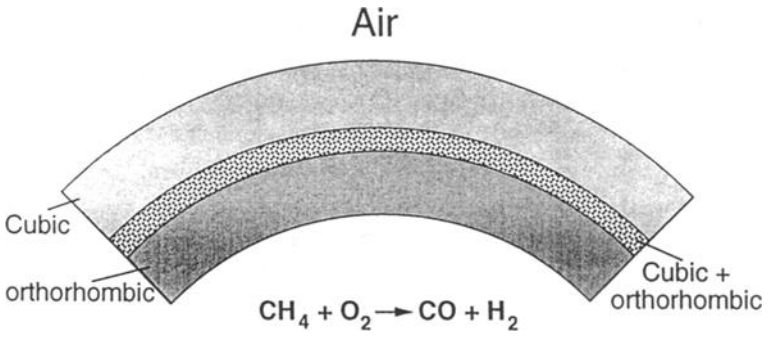

Fig. 8. Proposed phase representation for a membrane tube operated at a low flow rate of feed for synthesis gas generation.

match is generated across the membrane. Compared with the material on the outer wall, the material on the inner wall will elongate by an additional 1%, equivalent to the thermal expansion of about 350°C. We therefore believe that the strain associated with this lattice mismatch is the cause for the first type of fracture observed in the reaction tests.

On the other hand, we found that the second type of fracture arose from a different origin. XRD studies showed that the material in the outer shell, which was in contact with air, remained the same phase as the starting material. However, the material in the inner shell, which was in contact with the reaction stream, had decomposed. The decomposition products were the $SrCO_3$ phase and an iron phase (body-centered cubic), as shown in fig. 9. A separate Co phase (hexagonal) was not observed and it is expected that the iron phase observed may actually be a solid-solution of Co and Fe. Based on the lattice parameters of each phase, we found that the volume of the decomposed material was 30% larger than that of the starting material. As a result, a large crack, oriented parallel to the axis of the tube, was observed as shown in fig. 2.

The decomposition of membrane material is a direct result of the generation of H_2 and CO in the reaction stream. These products are highly reducing and tend to capture the oxygen in the membrane material at a fast rate. When there is no sufficient oxygen to replenish the vacancies via a permeation mechanism, a shell of decomposed material may form, as shown in fig. 10. The membrane will eventually crack due to the enormous expansion associated with the decomposition.

The occurrence of fracture in membrane reactors poses an urgent problem for the practical application of this technology for natural gas conversion. However, we feel that the problem could be overcome by control of the operating conditions and change of the reactor design and material. For example, to prevent the material from decomposition, the flow rate of the feed has to be controlled below a limit that the oxygen permeated from the air side is sufficient to replenish the oxygen vacancies created on the reaction side.

Although detailed discussion on the solution of the fracture problem falls out-

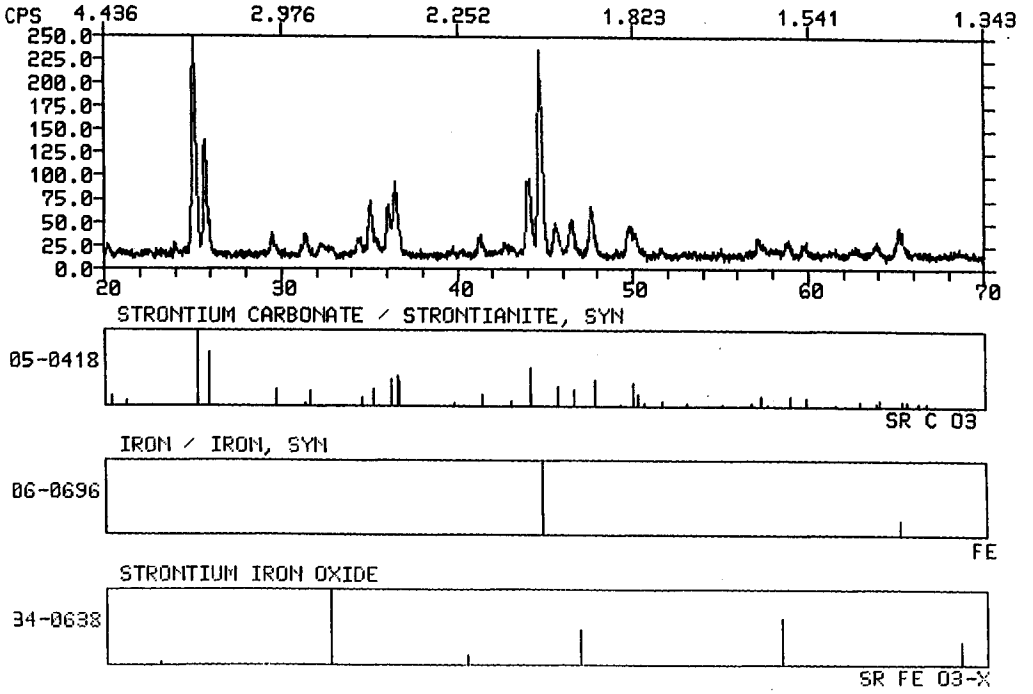

Fig. 9. XRD pattern taken at room temperature from the inner shell of the used reactor tube in fig. 2.

side the scope of this paper, we would like to point out that significant progress has already been made in the improvement of the lifetime of membrane reactors. Our recent runs lasted over a month without failure, compared with the earlier ones that lasted only for 1 h. Understanding of the failure mechanism in these membrane reactors has facilitated the process of improvement.

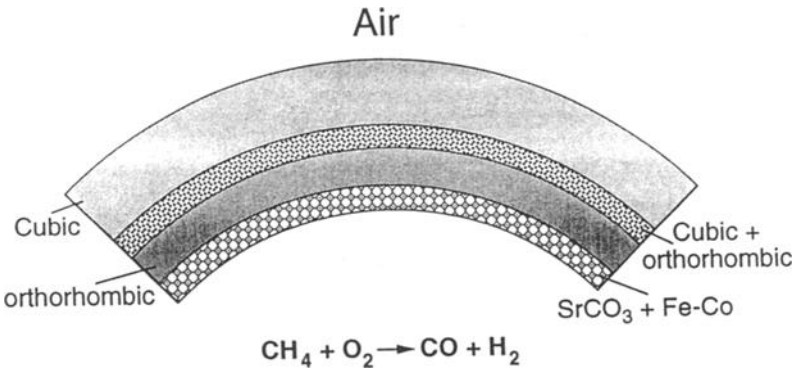

Fig. 10. Proposed phase representation for a membrane tube operated at a high flow rate of feed for synthesis gas generation.

4. Conclusions

(1) The fracture of the $Sr(Co_{0.8}Fe_{0.2})O_x$ tubes occurring shortly after initiation of the reaction is the consequence of a strain (or lattice mismatch) that is created by an oxygen gradient pointed from the reaction side to the air side. The oxygen gradient also leads to a phase change inside the membrane, which contributes to the build-up of strain.

(2) The failure of the $Sr(Co_{0.8}Fe_{0.2})O_x$ tubes occurring long after initiation of the reaction is caused by an enormous expansion of the membrane on the reaction side. The expansion arises from the decomposition of the membrane material in the presence of reducing reaction products of H_2 and CO.

(3) The whole $Sr(Co_{0.8}Fe_{0.2})O_x$ tube could have several shells, each having different phase constituents. The rate of oxygen permeation of the tube will be limited by the shell consisting of the least permeable material.

(4) Due to the change of the oxygen content at elevated temperature, the thermal expansion of $Sr(Co_{0.8}Fe_{0.2})O_x$ material tends to be unusually large.

Acknowledgement

We wish to thank G.W. Zajac of ARC for the coordination of early work and Y.-M. Chen and S. Short of ARC for technical support. We also thank T. Fleisch of the Alternative Feedstock Development Division, Amoco Corporation for guidance and support.

References

[1] G.E. Keller and M.M. Bhasin, J. Catal. 73 (1982) 9.
[2] G.J. Hutchings, M.S. Scurrell and J.R. Woodhouse, Chem. Soc. Rev. 18 (1989) 251.
[3] H.D. Gesser, N.R. Hunter and C.B. Prakash, Chem. Rev. 85 (1985) 235.
[4] N.D. Spencer and C.J. Pereira, J. Catal. 116 (1989) 399.
[5] G. Henrici-Olive and S. Olive, Angew. Chem. Int. Ed. Eng. 15 (1976) 136.
[6] Y. Teraoka, Hua-Min Zhang, S. Furukawa and N. Yamazoe, Chem. Lett. (1985) 1743.
[7] U. Blachandran, S.L. Morissette, J.T. Dusek, J.J. Picciolo, R.B. Poeppel, S. Pei, M.S. Kleefisch, R.L. Mieville, T.P. Kobylinski and C.A. Udovich, *Proc. Int. Gas Res. Conf.*, Orlando 16–19 November 1992.
[8] C. Greaves, A.J. Jacobson, B.C. Tofield and B.E.F. Fender, Acta Cryst. B 31 (1975) 641.
[9] M. Harder and H. Muller-Buschbaum, Z. Anorg. Allg. Chem. 464 (1980) 169.
[10] J. Mizusaki, M. Okayasu, S. Yamauchi and K. Fueki, J. Solid State Chem. 99 (1992) 166.
[11] J.C. Grenier, S. Ghodbane, G. Demazeau, M. Pouchard and P. Hagenmuller, Mater. Res. Bull. 14 (1979) 831.
[12] P.D. Battle, T.C. Gibb and P. Lightfoot, J. Solid State Chem. 76 (1988) 334.
[13] T. Hayakawa, H. Orita, M. Shimizu, K. Takehira, A. Anderson, K. Nomura and Y. Ujihira, Catal. Lett. 16 (1992) 359.

[14] H.M. Rietveld, J. Appl. Cryst. 2 (1969) 65.
[15] D.E. Gray, ed., *American Institute of Physics Handbook*, 3rd Ed. (McGraw-Hill, New York, 1972) p. 4-136.
[16] H. Kruidhof, H.J.M. Bouwmeester, R.H.E. van Doorn and A.J. Burggraaf, Solid State Ionics 63–65 (1993) 816.